Optical properties and phase-change transition in $Ge_2Sb_2Te_5$ flash evaporated thin films studied by temperature dependent spectroscopic ellipsometry

J. Orava[1*], T. Wágner[1], J. Šik[2], J. Přikryl[1], L. Beneš[3], M. Frumar[1]

[1]*Department of General and Inorganic Chemistry, Faculty of Chemical Technology, University of Pardubice, Cs. Legion's Sq. 565, Pardubice, 532 10 Czech Republic*
[2]*ON Semiconductor Czech Republic, R&D Europe, 1. máje 2230, Rožnov pod Radhoštěm, 756 61 Czech Republic*
[3]*Joint Laboratory of Solid State Chemistry of the Institute of Macromolecular Chemistry AS CR, v.v.i. and University of Pardubice, Studentská 84, Pardubice, 53210 Czech Republic*

[*]*Corresponding author: tel.: +420 466 037 220, fax: +420 466 037 311*
[*]*E-mail address: jiri.orava@upce.cz*

Keywords: $Ge_2Sb_2Te_5$, optical properties, ellipsometry, amorphous, fcc
PACs: 07.60.Fs, 77.84.Bw, 78.20.-e, 78.20.Bh

Abstract

We studied the optical properties of as-prepared (amorphous) and thermally crystallized (*fcc*) flash evaporated $Ge_2Sb_2Te_5$ thin films using variable angle spectroscopic ellipsometry in the photon energy range 0.54 - 4.13 eV. We employed Tauc-Lorentz model (TL) and Cody-Lorentz model (CL) for amorphous phase and Tauc-Lorentz model with one additional Gaussian oscillator for *fcc* phase data analysis. The amorphous phase has optical bandgap energy E_g^{opt} = 0.65 eV (TL) or 0.63 eV (CL) slightly dependent on used model. The Urbach edge of amorphous thin film was found to be ~ 70 meV. Both models behave very similarly and accurately fit to the experimental data at energies above 1 eV. The Cody-Lorentz model is more accurate in describing dielectric function in the absorption onset region. The thickness decreases ~ 7 % toward *fcc* phase. The bandgap energy of *fcc* phase is significantly lower than amorphous phase, E_g^{opt} = 0.53 eV. The temperature dependent ellipsometry revealed crystallization in the range 130 - 150 °C. The bandgap energy of amorphous phase possesses temperature redshift -0.57 meV/K (30 - 110 °C). The crystalline phase has more complex bandgap energy shift, firstly +0.62 meV/K (150 - 180 °C) followed by -0.29 meV/K (190 -

220 °C). The optical properties of as-prepared and *fcc* flash evaporated $Ge_2Sb_2Te_5$ thin films are very similar to those previously reported for sputtered thin films.

1. Introduction

The chalcogenide $Ge_2Sb_2Te_5$ thin film alloys are commercially used in optical phase change data storage media (DVD, blue-ray discs) and non-volatile phase change memories [1]. The wide application in DVD technology is mainly due to the fast phase change transition (~ 50 ns), highly repeatable cycles over 10^6 times and long lifetime of amorphous phase ~ 200 years. The main advantages of non-volatile phase change memories are fast programming time (< 10 ns), long-term data storage endurance exceeding 10^{13} programming operations and low voltage programming capability. This material is also very interesting in the field of cognitive computing [2]. Despite of the superior properties of $Ge_2Sb_2Te_5$ there are other potential materials, which could be used in the field of the phase change memory materials [3]. The $Ge_2Sb_2Te_5$ thin films are predominantly prepared by sputtering techniques, where structural [4], optical [5, 6] and electronic properties [7] have been widely investigated. The $Ge_2Sb_2Te_5$ thin films are regarded as *p*-type narrow-gap degenerated semiconductors, where the hole concentration increases toward crystalline phase [7]. As far as the authors know, no papers focused on ellipsometry study of flash evaporated $Ge_2Sb_2Te_5$ thin films have been published yet.

In this paper we present the optical function spectra of flash evaporated as-prepared (amorphous) and annealed (thermally crystallized, i.e., face-centered-cubic phase *fcc*) $Ge_2Sb_2Te_5$ thin films. The optical properties are studied by variable angle spectroscopic ellipsometry (VASE). We employed Tauc-Lorentz (amorphous and *fcc*) and/or Cody-Lorentz (amorphous) models to fit the optical parameters of studied films. The parameterization of models is also presented. We will show that the Tauc-Lorentz model with one additional Gaussian oscillator is well sufficient to describe the optical properties of crystalline $Ge_2Sb_2Te_5$ thin films. The temperature dependent ellipsometry was done to detect the phase change transition (amorphous to crystalline) and corresponding change of optical properties upon heating.

2. Experimental

$Ge_2Sb_2Te_5$ thin films with thickness ~ 200 nm were deposited from powdered bulk sample (grain size $\leq$ 0.4 mm) onto cleaned oxide glass substrates using flash evaporation technique (FE), which was developed at our laboratories. Deposition rate was kept at 0.3 nm/s and a

residual pressure of ~ 10^{-4} Pa. The crystalline phase was obtained by heating of the as-prepared films for 2 hours at 200 °C in N_2 atmosphere to avoid any surface oxidation.

The optical function spectra of the studied as-prepared and thermally crystallized thin films were evaluated from data measured using VASE® J. A. Woollam Co., Inc. ellipsometer with automatic rotating-analyzer (RAE) in the photon energy range from 0.54 to 4.13 eV, i.e., photon wavelengths 2300 - 300 nm, at angles of incidence 60°, 65° and 70°. The spectra were measured after 25 nm steps and the acquisition took about 30 minutes. The ellipsometer is equipped with AutoRetarder®, which allows the measurement of the ellipsometric parameter Δ at a 360° interval. The temperature dependent spectral ellipsometry was measured in the N_2 ambient in the temperature range 30 - 220 °C (303 - 493 K) in 10 °C step (around the crystallization with 5 °C steps). The sample was placed into HTC-100 heat cell developed by J. A. Woollam Co., Inc. and the spectra were taken throughout fused silica windows at fixed angle of incidence 70°. The phase change (PC) transition upon different heating rates (1 - 5 °C/min) was detected at one wavelength $\lambda = 1700$ nm (~ 0.73 eV), which is close to the optical bandgap energy of amorphous material and was found to be very sensitive for PC transition. The PC was done in the temperature range 30 - 200 °C.

X-ray diffraction data of thermally crystallized samples were obtained with a D8-Advance diffractometer (Bruker AXE, Germany) using CuKα radiation with secondary graphite monochromator.

AFM measurements were realized on Solver Pro M Atomic Force Microscope (NT-MDT; Russia) operating in semi-contact mode. The high-resolution „Golden" silicon cantilevers NSG-10 (Au coating, cone angle less than 22° and typical cantilever spring constant 11.5 $N.m^{-1}$) were used for all measurements. The images were recorded at engaged oscillation 50 % of free oscillation, scan frequency between 0.5 and 1 Hz for a resolution 256 x 256 pixel. The smoothness (S_a) was calculated according to ISO 4287-1997.

3. Theory

3.1 Spectroscopic Ellipsometry

Spectroscopic ellipsometry (SE) is known as an effective technique for determination of optical function spectra of variety of materials. The SE spectra are represented by traditional ellipsometry parameters Ψ and Δ, which denote the amplitude ratio and phase shift of perpendicularly polarized waves after their reflection off the surface of studied sample [8, 9]. The Ψ and Δ could be directly detected in nulling ellipsometry as an azimuthal angle of the

analyzer and polarizer at which the light intensity is minimal at the detector [8]. In RAE the time dependent flux $I(t)$ incident on detector for fixed polarizer element varies according to:

$$I(t) = I_0[1 + \alpha\cos 2A(t) + \beta\sin 2A(t)], \tag{1}$$

$$A(t) = 2\pi f_0 t + \theta, \tag{2}$$

where I_0 is the average intensity, α and β the normalized Fourier coefficients describing the phase and relative amplitude of the ac component of the flux incident on the detector. The Fourier coefficients α and β are measured in RAE. A represents immediate analyzer azimuth angle measured with respect to a zero reference. The A is a harmonic function of time, since the analyzer is rotating continuously. f_0 is an optical frequency, which equals to twice a mechanical rotation frequency and θ is an arbitrary constant phase factor [10]. If the detector signal is measured as function of time [Eqns. (1) and (2)] then the Fourier coefficients α and β of the signal could be obtained and the Ψ and Δ ellipsometry parameters in RAE calculated as follows

$$\alpha = \frac{\tan^2\Psi - \tan^2\Phi}{\tan^2\Psi + \tan^2\Phi}, \tag{3}$$

$$\beta = \frac{2\tan\Psi\cos\Delta\tan\Phi}{\tan^2\Psi + \tan^2\Phi}, \tag{4}$$

$$\tan\Psi = \sqrt{\frac{1+\alpha}{1-\alpha}}\left|\tan\Phi\right|, \tag{5}$$

$$\cos\Delta = \frac{\beta}{\sqrt{1-\alpha^2}}, \tag{6}$$

where Φ stands for polarizer azimuthal angle [11].

A common representation of the SE data Ψ and Δ is a complex pseudodielectric function $\langle\varepsilon\rangle = \langle\varepsilon_1\rangle + i\langle\varepsilon_2\rangle$, which eliminates the angle of incidence dependence of Ψ and Δ [12].

$$\langle\varepsilon\rangle = \langle\varepsilon_1\rangle + i\langle\varepsilon_2\rangle = \langle N\rangle^2 = \varepsilon_a\left[\left(\frac{1-\rho}{1+\rho}\right)^2\sin^2\Phi_a + \cos^2\Phi_a\right]\tan^2\Phi_a, \tag{7}$$

where N represents pseudocomplex refractive index. ε_a is the ambient dielectric function and equals 1 in case of air. An angle of incidence is denoted as Φ_a. The complex pseudodielectric function $\langle\varepsilon\rangle$ equals complex dielectric function ε only if ellipsometric data Ψ and Δ are measured from a bulk material with no layer on the top.

SE is an indirect technique and a model calculation is needed for sample analysis. Calculated model spectra are fitted to the experimental data by varying model parameters. Our model included surface roughness, thin film and oxide glass substrate. We did not involve any surface oxide layer into our models. As effective medium models are often used for modeling of microscopic surface roughness in spectroscopic ellipsometry [13], we modeled surface roughness by using the Bruggeman effective medium approximation (EMA), i.e., the surface layer consisting from the same bulk material with void density of 50 % [14]. The optical properties of bulk oxide glassy substrate were evaluated separately to reduce number of unknown parameters in the entire model. The Cauchy formula [9] was used to obtain a long-wavelength refractive index 1.4933 and curvature of refractive index toward higher energies 0.0083 in the entire spectral region, i.e., 300 - 2300 nm. The optical parameters of glassy substrate were kept constant during modeling process. We also did not include any correction to the free carrier absorption in this material, which gets significant at energies below measured region [15].

The number of unknown parameters for data analysis can be greatly reduced if an appropriate parameterization of optical functions, i.e., model dielectric functions (MDFs), is available for the materials of interest. A regression analysis is then used to differentiate the model parameters until the calculated (Ψ_i^{mod} and Δ_i^{mod}) and measured data (Ψ_i^{exp} and Δ_i^{exp}) match as closely as possible. This is performed by minimizing the mean square error function (MSE), which is appropriately weighted to the estimated experimental errors ($\sigma_{\Psi,i}^{exp}$ and $\sigma_{\Delta,i}^{exp}$).

$$\mathrm{MSE} = \sqrt{\frac{1}{2N-M}\sum_{i=1}^{N}\left[\left(\frac{\psi_i^{\mathrm{mod}}-\psi_i^{\mathrm{exp}}}{\sigma_{\psi,i}^{\mathrm{exp}}}\right)^2 + \left(\frac{\Delta_i^{\mathrm{mod}}-\Delta_i^{\mathrm{exp}}}{\sigma_{\Delta,i}^{\mathrm{exp}}}\right)^2\right]}. \tag{8}$$

The number of measured ψ and Δ pairs is N and the total number of real valued fit parameters is M. For detailed information on the principal of ellipsometry we refer to [8, 9 and 11].

3.2 MDFs (model dielectric functions) of FE Ge$_2$Sb$_2$Te$_5$ thin films

The optical functions are usually in the form of a complex dielectric function $\varepsilon = \varepsilon_1 + i\varepsilon_2$ or a complex refractive index $N = n + ik$, where n is refractive index (real part) and k extinction coefficient (imaginary part) and $\varepsilon = N^2$ Eq. (7). The real and imaginary part of complex dielectric function and refractive index are connected throughout $\varepsilon_1 = n^2 - k^2$ and $\varepsilon_2 = 2nk$. We used two following dispersion models, i.e., Tauc-Lorentz (TL) [16, 17] and Cody-Lorentz (CL) [18] to obtain optical functions of the studied samples in the entire measured region. One additional Gaussian oscillator (G_{osc}) [11] was added into TL model to describe the more pronounced structure of dielectric function of crystalline sample. The above mentioned models (TL, TL + G_{osc}) were also used to evaluate the varying of optical function spectra of $Ge_2Sb_2Te_5$ thin films in dependence on temperature [19].

The Tauc-Lorentz model

The Tauc-Lorentz (TL) oscillator model developed by Jellison and Modine [16, 17] was used to describe the optical functions of amorphous films in the entire measured spectral region. Using the same model with additional Gaussian oscillator (TL+G_{osc}) we obtained the optical functions of the studied *fcc* $Ge_2Sb_2Te_5$ thin films. We also made a report on the oscillator parameters extracted from TL model. The ε_2 imaginary part of dielectric function according to the TL model is obtained by taking into account Tauc joint density of states [20], Lorentz oscillator [11] and Forouhi and Bloomer formalism [21, 22] of optical function. The following dispersion is obtained

$$\varepsilon_{2TL}(E) = 2nk = \frac{(E - E_g^{opt})^2}{E^2} \cdot \frac{ACE_0E}{(E^2 - E_0^2)^2 + C^2E^2} = G(E)L(E).$$ (9)

$G(E)$ and $L(E)$ represent variable band-edge function and Lorentz oscillator function, respectively. The $G(E)$ represents here the Tauc law, i.e., $\hbar\omega^2\varepsilon_2 \sim (\hbar\omega - E_g^{opt})^2$. The parameters in Eq. (9) are amplitude (oscillator strength) A, peak transition energy E_0, optical bandgap energy E_g^{opt} and broadening C. The Eq. (9) is used in the range of energies $E > E_g^{opt}$. $\varepsilon_{2Tauc-Lorentz}$ is 0 in the range of energies $E \leq E_g^{opt}$, i.e., below optical bandgap energy. This model contains only interband transitions. Some defects and/or intraband transitions are not included in this model. The real part of dielectric function ε_1 is calculated by the Kramers-Kronig integration formula

$$\varepsilon_1(E) = \varepsilon_1(\infty) + \frac{2}{\pi} P \int\limits_{E_g^{opt}}^{\infty} \frac{\xi \varepsilon_2(\xi)}{\xi^2 - E^2} d\xi, \qquad (10)$$

where P stands for the Cauchy principal part of the integral. $\varepsilon_1(\infty)$ is a fitting parameter in the model and represents constant contribution to ε_1 at high energies beyond the measured spectral region. The integral could be solved in the closed form which is shown elsewhere [16, 17].

The Cody-Lorentz model

The Cody-Lorentz (CL) oscillator model was developed by Ferlauto *et al.* [18]. It is similar to TL in the way that it defines E_g^{opt} and Lorentz absorption peak. However the $G(E)$ behaves differently in the absorption onset region and Urbach absorption term is also included.

$$\varepsilon_{2CL} = \begin{cases} \dfrac{E_1}{E} \exp\left(\dfrac{E - E_t}{E_u}\right); & 0 < E \leq E_t \qquad (11a) \\[4mm] G(E)L(E) = \dfrac{(E - E_g^{opt})^2}{(E - E_g^{opt})^2 + E_p^2} \cdot \dfrac{ACE_0 E}{(E^2 - E_0^2)^2 + C^2 E^2}; & E > E_t, \qquad (11b) \end{cases}$$

where E_t is the boundary between Urbach tail transition, which forms the top of valence band and the band-to-band transition. In Eq. (11a) the expression for $0 < E \leq E_t$ leads to the Urbach form of the absorption coefficient, i.e., $\alpha(E) \sim exp(E/E_u)$ [23]. E_u is corresponding weak Urbach absorption energy. The E_1 is defined so that $\varepsilon_{2CL}(E)$ is continuous at $E = E_t$; thus $E_1 = E_t L(E_t)G(E_t)$. E_p in Eq. (11) defines a second transition energy (in addition to E_t), that separates the absorption onset behavior $E < E_p + E_g^{opt}$ from Lorentz oscillator behavior $E > E_p + E_g^{opt}$. The other parameters A, C, E_0 and E_g^{opt} in Eq. (11b) have the same meaning as in Eq. (9). The real part of dielectric function ε_1 is again given by Kramers-Kronig integral Eq. (10).

Additional Gaussian Oscillator

The TL dispersion model was extended by using one additional Gaussian oscillator (G_{osc}) [11] to predict the optical function spectra of crystalline phase. The additional G_{osc} oscillator

helps describe the sharper behavior of ε_2 in crystalline phase contrary to amorphous one. The imaginary part of dielectric function of Gaussian oscillator is given as follows

$$\varepsilon_{2G_{osc}}(E) = \frac{A_G}{C_G}\exp^{-\left(\frac{E-E_G}{C_G}\right)^2} + \frac{A_G}{C_G}\exp^{-\left(\frac{E+E_G}{C_G}\right)^2}.$$ (12)

The A_G, E_G ($E_G \sim E_0$) and C_G have the same meaning as in Eqns. (9) and (11b) . The subscript in the parameters is used to distinguish the additional G_{osc} parameters from the main dispersion coefficients of TL model. The real part of dielectric function of Gaussian oscillator is calculated throughout KK integral [Eq. (10)]. It has to be pointed out that further in the text the $\varepsilon_1(\infty)$ from Eq. (10) represents summary of total constant contributions to ε_1 from TL and G_{osc} in the case of crystalline phase. The final dielectric function of studied Ge$_2$Sb$_2$Te$_5$ (*fcc*) is then given as follows $\varepsilon_1 = \varepsilon_1(\infty) + \varepsilon_{1TL} + \varepsilon_{1Gosc}$ and in the same way the $\varepsilon_2 = \varepsilon_{2TL} + \varepsilon_{2Gosc}$.

4. Results

The composition of FE as-prepared Ge$_2$Sb$_2$Te$_5$ thin films determined by EDAX analysis was 22.6 at. % Ge, 24.1 at. % Sb and 53.3 at. % Te, which is very close to a nominal composition of bulk sample (Ge$_{22.2}$Sb$_{22.2}$Te$_{55.6}$). The accuracy of EDAX is ± 0.5 at. %. The comparison of experimental and modeled pseudodielectric functions according to TL and CL model of four layers system ambient/roughness/amorphous thin film/glassy substrate is depicted in Figs. 1a (real part) and 1b (imaginary part). The inserted figures show detail look at the regions near and below the optical bandgap energy. Both models show very good agreement with the experimental data. It is seen that in $<\varepsilon_1>$ the CL data matches the experimental data better than TL in the absorption onset (Fig. 1a). The calculated parameters of both TL and CL models are listed in Tab. 1. The errors presented in Tab. 1 are statistical errors and refer to uncertainty of the final value of the parameter. It is defined as 90 % probability that the true parameter value lies inside the interval. The comparison of calculated ε_2 according to TL and CL models is shown in Fig. 2. The logarithmic scale of ε_2 vs. *energy* is preferred to cover the entire spectral region. There is no difference in ε_2 at high photon energies. Significant difference might be seen below the $E_t = 0.79$, where TL model follows Tauc law resulting in sharp decrease in ε_2 below the bandgap energy. On the other hand CL posses gentle onset of absorption edge as it contains the localized states above the valence band given by Urbach energy $E_u \sim 70$ meV (Tab. 1). The bandgap energy is slightly

dependent on used model, where $E_g^{opt} = 0.65$ eV (TL) and $E_g^{opt} = 0.63$ eV (CL). It should be noted that both models resulted in the same value of film thickness (~ 195 nm) and surface roughness (~ 6 nm) according to EMA layer (Tab. 1). In agreement with the same ε_2 at higher energies, the calculated TL and CL peak position E_0 and peak broadening C have very similar values (Tab. 1). The amplitude A in CL model has lower value than in TL as it compensates different $G(E)$ function in Eqns. (9) and (11).

The good agreement between experimental and modeled pseudodielectric function of crystalline $Ge_2Sb_2Te_5$ in the entire spectral region is depicted in Figs. 3a and 3b. There is a significant decrease in the optical bandgap energy E_g^{opt} from 0.65 eV to 0.53 eV and main TL parameters, i.e., peak broadening C (from 3.91 eV to 2.13 eV) and peak position E_0 (2.55 eV to 1.32 eV) contrary to amorphous phase (Tab. 1). On the other hand the peak amplitude increased from 114 eV to 181 eV. This increase is also accompanied by higher values of ε_2 around E_0 in crystalline phase contrary to amorphous one (Fig. 4b). The ε_2 maximum is determined by amplitude contributions from Lorentz oscillator, Eq. (9) and additional Gaussian oscillator, Eq. (12). The Fig. 4 shows calculated values of ε_1 and ε_2 of studied samples. The inserted figures show the behavior of refractive index n and extinction coefficient k. The observed thickness decrease was ~ 7 % from amorphous to crystalline (from 195 nm to 181 nm). The MSE error of *fcc* phase is distinctively higher without using one additional Gaussian oscillator in the entire model MSE ~ 4. Without using the Gaussian oscillator a significant difference between experimental and modeled data could be found at ~ 1 eV photon energy and above. Adding additional oscillator at photon energy ~ 1.8 eV helps to overcome this experimental to model data discrepancy. Kato *et al.* [7] showed that the absorption spectra of *fcc* phase could be more satisfactory fitted by indirect absorption formula $\alpha\hbar\omega \sim (\hbar\omega - E_g^{opt})^2$ than by direct, where $\alpha\hbar\omega \sim (\hbar\omega - E_g^{opt})^{1/2}$. The former equation gave us $E_g^{opt} = 0.48$ eV, which is very close to our TL optical bandgap energy 0.53 eV. The direct interband transition formula resulted in $E_g^{opt} = 1.67$ eV (Fig. 5).

The differences (errors) between experimental and modeled pseudodielectric spectra of amorphous and crystalline phases are depicted in Fig. 6a (amorphous - Tauc-Lorentz model), Fig. 6b (amorphous - Cody-Lorentz model) and Fig. 6c (crystalline - Tauc-Lorentz + Gaussian oscillator model). The deeper look at the region around the bandgap energy of amorphous phase TL vs. CL is depicted separately in Fig. 7 for $\langle\varepsilon_1\rangle$ (Fig. 7a) and $\langle\varepsilon_2\rangle$ (Fig. 7b). The difference between experimental and modeled data is slightly lower in the case of CL model than those fitted by TL around the bandgap energy (Figs. 7a and 7b).

The XRD spectra of as-prepared (amorphous) and thermally crystallized (annealed at 220 °C) $Ge_2Sb_2Te_5$ thin films are shown in Fig. 8. The *hkl* parameters of *fcc* phase could be assigned according to Yamada *et al.* [24], where (111) 2θ = 25.59°, (200) 2θ = 29.63°, (220) 2θ = 42.40° and (222) 2θ = 52.58°. The AFM surface roughness of studied samples was found to be lower than the optical surface roughness calculated from ellipsometry. The former method gave us surface roughness 2.6 nm (amorphous) and 5.7 nm (*fcc*), respectively. The surface roughness calculated from ellipsometry was 6 nm and for amorphous and 7.5 nm for crystalline phase. Higher ellipsometry values may mean that EMA layer accounts for surface roughness as well as few nanometers of oxide layer. It is supposed that GeSbTe ternary alloys might be subject to long time oxidation, nevertheless details are not known [7].

The temperature dependent ellipsometry, i.e., behavior of Ψ and Δ upon heating is depicted in Fig. 9 at λ = 1700 nm. The contribution of bulk oxide glassy substrate to the change of Ψ and Δ could be considered as negligible, i.e., the change of substrate in Ψ was detected to be ~ 0.1 deg and in Δ ~ 0.3 deg in the temperature range 30 - 300 °C. The small change in Ψ and Δ is followed by very slight change of long wavelength refractive index at third decimal place, which is the detection limit of the temperature dependent spectral ellipsometry measurement. The abrupt change in Ψ and Δ in the temperature range 130 - 150 °C is due to the phase change transition (amorphous to crystalline) occurring in the $Ge_2Sb_2Te_5$ thin films. The phase change transition shifts towards higher temperatures with increasing heating rate, i.e., 1 °C/min, 2.5 °C/min and 5 °C/min. The Fig. 10 shows the temperature dependence of refractive index on temperature as calculated from Fig. 9 (2 °C/min, λ = 1700 nm). The maximal error in determination of refractive index of $Ge_2Sb_2Te_5$ thin films at the single wavelength ellipsometry was ± 0.04. The Fig. 10 also shows temperature derivation of *dn/dT*. The spectrum has been taken as single wavelength ellipsometry at λ = 1700 nm with repeating cycle of one point ~ 6 s.

The temperature dependent spectral ellipsometry (300 - 2300 nm) was done to calculate the absorption edge shift of amorphous and crystalline phases (Fig. 11). The absorption edge of amorphous phase shows linear redshift with coefficient -0.57 meV/K, in the temperature range 30 - 120 °C. The crystalline phase possesses more complex change of short-wavelength absorption edge. In the temperature range 150 - 180 °C we obtained +0.62 meV/K and 190 - 220 °C -0.29 meV/K shift of optical bandgap energy. The Tauc-Lorentz model was used to obtain the bandgap shift in the temperature range 30 - 120 °C. The bandgap shift in temperature range 150 - 180 °C and 190 - 220 °C was calculated using combination of Tauc-Lorentz with one additional Gaussian oscillator. The characteristic averages MSE for one

10

angle fits (70°) in the entire spectral region are ~ 3.9 in the case of amorphous phase and ~ 1.0 for crystalline phase.

5. Discussion

The both presented models, i.e., Tauc-Lorentz and Cody-Lorentz are able to describe the dielectric function of flash evaporated amorphous $Ge_2Sb_2Te_5$ thin films (Figs. 1 and 2). They possess overall good agreement between experimental and modeled data in the entire spectral region. Both models behave similarly at higher energies, i.e., ~ 1.5 eV up to 4.13 eV. This region is governed by the same Lorentz oscillator formula $L(E)$ in both models [Eqns. (9) and (11b)]. Both TL and CL Lorentz function resemble in the peak broadening C and position E_0 (Tab. 1). The main difference is in the amplitude A, where $L(E)$ compensates different magnitude of $G(E)$ in Eqns. (9) and (11b). First distinguished difference in the ε_2 spectra (Fig. 2) is seen at $E_g^{opt} + E_p = 1.18$ eV (Tab.1). In the CL model this region separates the behavior of absorption onset from Lorentz oscillator behavior. This so called second transition provides higher flexibility for absorption shape modeling of CL model contrary to TL model [16, 17 and 18]. The outstanding discrepancy in TL and CL ε_2 spectra is at first transition energy $E_t = 0.79$ eV (Fig. 2), which corresponds to demarcation energy between the Urbach tail transition and the band-to-band transition in material according to CL model [Eq. (11a)] [18]. Below this region (0.79 eV) the TL starts to drop sharply at $\varepsilon_2 = 0$ resulting in bandgap energy $E_g^{opt} = 0.65$ eV (Tab. 1), i.e., the TL model does not describe any weak absorption tail bellow the bandgap energy [Eq. (9)]. On the other hand CL follows Eq. (11a) in the spectral region $0 < E \leq E_t$. The corresponding $E_g^{opt} = 0.63$ eV and $E_u = 70$ meV were calculated (Tab. 1) at room-temperature. The CL matches better to the experimental data around and below the bandgap energy as it is seen from the difference plot between $<\varepsilon_1>$ and $<\varepsilon_2>$ experimental vs. modeled data in Figs. 6a, 6b and Figs. 7a and 7b. The found values of E_g^{opt} and E_u of amorphous phase are in good agreement with those reported in [7]. The authors found optical bandgap energy of DC sputtered amorphous $Ge_2Sb_2Te_5$ thin films $E_g^{opt} = 0.74$ eV and Urbach energy ~ 50 meV from transmission spectra using Tauc plot [20], respectively. Ju *et. al* [25] reported Urbach edge ~ 40 and/or ~ 90 meV in dependence on sputtering deposition rate. Value of bandgap energy 0.7 eV (TL) and Urbach edge ~ 81 meV was reported by Lee *et. al* [26]. It should be noted that the optical properties of sputtered thin films vary dramatically with deposition conditions [5]. The bandgap energy of FE thin films is close to pulsed laser deposited amorphous $Ge_2Sb_2Te_5$ thin films, where $E_g^{opt} = 0.79$ eV according to PDOS model [27]. The better fit of CL model to experimental data is also represented by lower MSE =

1.937 contrary to TL model MSE = 2.476. We might expect that the CL model is favorable for amorphous $Ge_2Sb_2Te_5$ thin films. The defects which are represented by non-zero absorption below E_g^{opt} occur naturally in these materials. The defects appear as localized states above the valence band in density of states (DOS), i.e., Urbach edge is governed by the valence band tail [28]. It might be plausible to consider these localized states as results of "wrong" covalently bound atoms in amorphous chalcogenides, i.e., so called valence alternation pairs (VAPs) [29, 30 and 31]. Some studies suggested that the VAPs defects might be created due to the over-coordinated 3-fold Te atoms as it was shown in EXAFS studies [32, 33], since their normal valency is 2-fold. The 3-fold Te^+ is then positively charged. The negative charge is then assumed to be located at 3-fold Ge atoms and/or 2-fold Sb atoms, i.e., forming Ge^- and/or Sb^- charged centers [34, 35 and 36]. It should be noted that the problem is still under deep study of many researchers and the VAPs model its self seems to be more complicated in the case of telluride glasses [37] than it was proposed, e.g., for sulfide and/or selenide glasses [31].

The $Ge_2Sb_2Te_5$ crystalline phase shows more pronounced structure of dielectric function spectra contrary to amorphous state (Fig. 4). The sharper shape has been modeled by using Tauc-Lorentz dispersion formula with additional Gaussian oscillator (Fig. 3). It is not possible to employ the CL model in crystalline phase. This is mainly due to the impossibility to model the Urbach edge in highly ordered crystalline phase contrary to amorphous one. The TL model is also favorable as it has lesser number of varying parameters. The TL model except of its wide use in amorphous semiconductors is also very acceptable for describing optical properties of indirect crystalline semiconductors as it was, e.g., shown for polycrystalline bismuth selenotelluride thin films [38] and GeSbTe thin film alloys [39]. Other authors applied multiple Lorentz oscillators [11] to describe the dielectric function of meta-stable *fcc* phase [26, 40]. Older studies also applied Cauchy model [11] to describe *n* and *k* of $Ge_2Sb_2Te_5$ sputtered thin films [41]. The MSE error of TL model without using one additional Gaussian oscillator was ~ 4. The Gaussian oscillator (MSE = 0.998) might be replaced by classical Lorentz oscillator, i.e., MSE ~ 1.1. The Lorentz oscillator has shallower peak behavior resulting in ineligible small absorption tail below the bandgap energy. It is of high interest that the position of Gaussian oscillator E_G = 1.77 eV (Tab. 1) is very close to the direct transition $E_g^{opt}(direct)$ = 1.67 eV (Fig. 5) calculated from linear region of $(\alpha E)^2$ vs. *energy* plot. Therefore the Gaussian oscillator is assumed to be connected with direct transition in *fcc* $Ge_2Sb_2Te_5$ thin films. The valence band of thermally crystallized $Ge_2Sb_2Te_5$ is dominated by Te, Ge and Sb p states with minor contribution from s states of Ge and Sb.

The conduction band is mainly populated by anti-bonding p states of Ge, Sb and p states of Te [42]. The peak at 1.77 eV might be assigned to the transitions between Te p bonding and Ge/Sb p anti-bonding states. Nevertheless the precise determination of the states involved in this transition is not possible. As we mentioned in the literature data the either TL [39] or multiple Lorentz oscillators [26, 40] are used to evaluate dielectric function of sputtered *fcc* thin films. The combination of TL + G_{osc} or other type of oscillators as far as we know have not been published yet for sputtered thin films. It seems to be necessary to consider further studies of FE thin films with regard to: 1) Is the additional oscillator characteristic only for FE *fcc* thermally crystallized thin films? and 2) Is the additional oscillator needed also for laser crystallized FE thin films? Our preliminary experiments on the optically crystallized FE $Ge_2Sb_2Te_5$ thin films show significant difference in behavior of laser crystallized contrary to thermally crystallized materials and also different approach in evaluating ellipsometry spectra is needed. The additional oscillator seems to be also important for laser crystallized thin films and it is plausible to take into account Lorentz oscillator rather than Gaussian oscillator. The problem is still under study. Just to be noted that Yamanaka *et. al* [43] modeled underestimated transition in hexagonal sputtered $Ge_2Sb_2Te_5$ at 1.2 eV (experimental value ~ 1.8 eV). This peak has been supposed to arise due to the Te p to Sb p transitions. The current consensus supposes that the meta-stable $Ge_2Sb_2Te_5$ *fcc* structure posses the rocksalt like structure, which belongs into the space group Fm-3m [24]. One site (4a) of the lattice is fully occupied by only Te atoms and the other site (4b) is randomly occupied by Ge/Sb mixing and 20 % of vacancies. [24]. The lattice parameter of ~ 6 Å has been reported for thermally crystallized thin films [42]. Kolobov *et. al* proposed that $Ge_2Sb_2Te_5$ does not posses rocksalt structure but more likely consists of well-defined rigid building blocks that are randomly oriented in space consistent with cubic symmetry [33]. The decrease in position of the Lorentz peak E_0 from 2.55 eV to 1.32 eV (amorphous to crystalline) might be caused by increase in medium-range order (MRO) of crystalline phase [44]. This MRO change is also accompanied by decrease in peak broadening *C* from ~ 3.9 eV to ~ 2.1 eV (Tab. 1). The found value of crystalline bandgap energy 0.53 eV is in good agreement with ~ 0.5 eV reported in [7, 26 and 27]. It should be noted that the found bandgap energy of crystalline phase is at the edge of our spectral region. Still the accurate calculation of the bandgap energy could be done with respect to accurate model data and measuring the most part of absorption onset region (Figs. 1, 3, 7 and 8). Weidenhof *et al.* [45] published 6 % decrease in volume upon crystallization. We found ~ 7 % thickness depression upon crystallization (Tab. 1). The thickness (volume) change is expected as the amorphous phase has larger free volume than the crystalline phase.

The phase change transition from amorphous to crystalline state shows significant change in the Ψ and Δ spectra (Fig. 9) and corresponding change of refractive index (Fig. 10). The crystallization takes place between 130 - 150 °C. Just to be noted that at one measured wavelength the corresponding refractive index and film thickness are strongly correlated. The change of refractive index (Fig. 10) was fitted using point-by-point technique, where every point is fitted separately regardless of any dispersion formula [Eqs. (9), (10) and (11)]. The only fitting parameter was refractive index. The thickness was set to constant value of amorphous phase ~ 195 nm. This fitting procedure led to lower absolute value of refractive index of crystalline phase as the thickness was kept constant, i.e., Δn ~ 0.2 (2.8 %), at λ = 1700 nm and 200 °C. The fitting procedure does not affect the overall behavior of refractive index as well as the abrupt change due to the crystallization. The resulting MSE of point-by-point fit was 0.274. It has been shown that $Ge_2Sb_2Te_5$ thin films may crystallize even at temperatures ~ 110 °C [46] with grains size ~ 3 nm. This grain size is beyond our detection limit. If we think about the 1 °C/min in first approximation as an "isothermal" measurement, the first and second peaks might be assigned to the fast nucleation process followed by slower grain growth during the thermal treatment [47, 48]. On the other hand the complex behavior might be due to the coexistence of more crystallographic structures not only of the dominated *fcc* phase [49] and/or phases separation could occur. More phases are also supposed to exist in laser crystallized films, where amorphous phase around *fcc* grains are expected to coexist together [24, 50]. The different lattice parameters and/or crystallization and/or separation of different phases are favorable as the thermal treatment is slow and processes with higher energy barrier may rise after longer time. The idea of two parallel processes might be also supported by two significant peaks in *dn/dt* plot (Fig. 10). The optical bandgap of amorphous phase shifts linearly with slope -0.57 meV/K (Fig. 11), which is in good agreement with value found for sputtered films [7]. The bandgap shifts with +0.62 meV/K up to 180°C after the crystallization has been finished (Figs. 9 and 10). It is of high interest that the slope has almost the same value but inverse slope in comparison with amorphous state. The bandgap energy shows again redshift above the 190 °C with slope -0.29 meV/K, which is in good agreement with [7]. This might be also connected with multi phase crystallization processes upon thermal treatment, nevertheless the more complex behavior of the bandgap energy in the crystalline phase is not understood and needs to be studied further.

6. Conclusion

We have showed that both Tauc-Lorentz and Cody-Lorentz models can sufficiently describe the dielectric function of flash evaporated $Ge_2Sb_2Te_5$ thin films in the 0.54 - 4.13 eV photon energy region. Both models led to the same dielectric constants at energies above 1 eV. The Cody-Lorentz model seems to be more accurate for modeling of the absorption onset region. The main advantage of CL model is that it contains absorption on defects states such as valence alternation pairs, which are very favorable in chalcogenide thin films. The bandgap energies of as-prepared (FE) thin films were calculated 0.65 eV (TL) and 0.63 eV (CL), respectively and the Urbach edge was estimated to be ~ 70 meV. It is also shown that the optical properties of as-deposit flash evaporated thin films are in very good agreement with those reported for sputtered thin films.

The dielectric function of fcc $Ge_2Sb_2Te_5$ FE thin films might be very accurately defined by Tauc-Lorentz model + one additional Gaussian oscillator. The bandgap energy of fcc phase was estimated 0.53 eV. The TL bandgap energy is similar to the indirect bandgap energy calculated from linear plot of $(\alpha\hbar\omega)^{1/2}$ vs. *energy*, where E_g^{opt} = 0.48 eV. The position of Gaussian oscillator is very close to the direct interband transition in crystalline phase 1.67 eV. This peak has been assumed to arise due to the transitions between Te p bonding and Ge/Sb p anti-bonding states. We found ~ 7 % decrease in thickness and ~ 50 % decrease in Lorentz peak position and broadening toward crystalline phase. The decrease in peak parameters might be assigned to decrease in disorder in crystalline phase contrary to amorphous one. The optical properties of fcc FE $Ge_2Sb_2Te_5$ are also very similar to corresponding sputtered thin films.

The temperature dependent ellipsometry showed that the crystallization upon temperature starts at ~ 130 °C and is finished at ~ 150 °C. The bandgap shift in amorphous phase is -0.57 meV/K (30 - 120 °C). The bandgap shift in crystalline phase is more complicated, the increase +0.62 meV/K (150 - 180 °C) is followed by -0.29 meV/K in temperature range 190 - 220 °C. It is suggested that the thermal treatment induced multi phase crystallization consisting of at least two parallel processes, dominated by occurrence of fcc phase. The further studies are necessary.

References

[1] S. R. Ovshinsky, Application of Non-Crystalline Materials, in *Insulating and Semiconductor Glasses*, edited by P. Boolchand (World Scientific Publishing Co. Pte. Ltd., Singapore, 2000), pp. 729-779.

[2] S. R. Ovshinsky, B. Pashmakov, Mat. Res. Soc. Symp. Proc. **803**, HH1.1.1. (2004).

[3] M. Frumar, B. Frumarova, T. Wagner, M. Hrdlicka, J Mater Sci: Mater Electron **18**, S169 (2007).

[4] S. Kohara, K. Kato, S. Kimura, Hit. Tanaka, T. Usuki, K. Suzuya, Hir. Tanaka, Y. Moritomo, T. Matsunaga, N. Yamada, Y. Tanaka, H. Suematsu, M. Takata, Appl. Phys. Lett. **89**, 201910 (2006).

[5] H. Dieker, M. Wuttig, Thin Solid Films **478**, 248 (2005).

[6] T. Ohta, S. R. Ovshinsky, Phase-Change Optical Storage Media, in *Photo-Induced Metastability in Amorphous Semiconductors*, edited by A. V. Kolobov (Wiley-VCH, Weinheim, 2003), pp. 310-326.

[7] T. Kato, K. Tanaka, Jpn. J. Appl. Phys. **44**, 7340 (2005).

[8] R. M. A. Azzam and N. M. Bashara, *Ellipsometry and Polarized Light* (North-Holland, Amsterdam, 1984).

[9] H. G. Tompkins, W. A. McGahan, *Spectroscopic Ellipsometry and Reflectometry* (Wiley Inter-Science, New York, 1999).

[10] D. E. Aspnes, A. A. Studna, Appl. Opt. **14**, 220 (1975).

[11] H. G. Tompkins, E. A. Irene, *Handbook of Ellipsometry* (William Andrew, Inc., New York, 2005).

[12] D. E. Aspnes, A. A. Studna, Phys. Rev. B **27**, 98 (1983).

[13] D. E. Aspnes, J. B. Theeten, F. Hottier, Phys. Rev. B **20**, 3292 (1979).

[14] D. A. G. Bruggeman, Ann. Phys. 24 (1935) 636.

[15] A. Mendoza-Galvan, J. Gonzalez-Hernandez, J. Appl. Phys. **87**, 760 (2000).

[16] G. E. Jellison, Jr., F. A. Modine, Appl. Phys. Lett. **69**, 371 (1996).

[17] G. E. Jellison, Jr., F. A. Modine, Appl. Phys. Lett. **69**, 2137 (1996).

[18] A. S. Ferlauto, G. M. Ferreira, J. M. Pearce, C. R. Wronski, R. W. Collins, X. Deng, G. Ganguly J. Appl. Phys. **92**, 2424 (2002).

[19] N. F. Mott, E. A. Davis, *Electronic Processes in Non-Crystalline Materials* (Clarendon Press, Oxford, 1971).

[20] J. Tauc, R. Grigorovic, A. Vancu, Phys. Stat. Sol. **15**, 627 (1966).

[21] A. R. Forouhi, I. Bloomer, Phys. Rev. B **34**, 7018 (1986).

22. A. R. Forouhi, I. Bloomer, Phys. Rev. B **38**, 1865 (1988).

23. J. Tauc, Optical Properties of Non-Crystalline Solids, in *Optical Properties of Solids*, edited by F. Abeles (North-Holland Publishing Company, Amsterdam, 1972), pp. 278-313.

24. N. Yamada, T. Mastunaga, J. Appl. Phys. **88**, 7020 (2000).

25. T. Ju, J. Viner, H. Li, P. C. Taylor, J. Non-Cryst. Solids (2008), doi:10.1016/j.jnoncrysol.2007.10.088.

26. Bong-Sub Lee, J. R. Abelson, S. G. Bishop, Dae-Hwan Kang, Byung-ki Cheong, Ki-Bum Kim, J. Appl. Phys. **97**, 093509 (2005).

27. D. Franta, M. Hrdlicka, D. Necas, M. Frumar, I. Ohlidal, M. Pavlista, Phys. Stat. Sol. (c) **1-4** (2008), doi:10.1002/pssc.200777768.

28. K. Tanaka, J. Optoelectron. Adv. Mater. **3**, 189 (2001).

29. H. Fritzsche, J. Phys. Chem. Solids **68**, 878 (2007).

30. M. Popescu, Structure, Defects and Electronic Properties of Amorphous Semiconductors, in *Photo-Induced Metastability in a-Semiconductors*, edited by A. V. Kolobov (WILEY-VCH, Weinheim, 2003), pp. 1-20.

31. J. Singh, K. Shimakawa, Defects, in: *Advances in Amorphous Semiconductors* (Taylor & Francis, London, 2003), pp. 158-203.

32. D. A. Baker, M. A. Paesler, G. Lucovsky, P. C. Taylor, J. Non-Cryst. Solids **352**, 1621 (2006).

33. A. V. Kolobov, P. Fons, A. I. Frenkel, A. L. Ankudinov, J. Tominaga, T. Uruga, Nat. Mater. **3**, 703 (2004).

34. M. A. Paesler, D. A. Baker, G. Lucovsky, A. E. Edwards, P. C. Taylor, J. Phys. Chem. Solids **68**, 873 (2007).

35. D. A. Baker, M. A. Paesler, G. Lucovsky, S. C. Agarwal, P. C. Taylor, Phys. Rev. Lett. **96**, 25551 (2006).

36. G. Lucovsky, D. A. Baker, M. A. Paesler, J. C. Philips, J. Non-Cryst. Solids **353**, 1713 (2007).

37. J. Robertson, K. Xiong, P. W. Peacock, Thin Solid Films **515**, 7538 (2007).

38. A. Zimmer, N. Stein, H. Terryn, C. Boulanger, J. Phys. Chem. Solids **68**, 1902 (2007).

39. A. Chabli, C. Vergnaud, F. Bertin, V. Gehanno, B. Valon, B. Hyot, B. Bechevet, M. Burdin, D. Muyard, J. Magn. Magn. Mater. **249**, 509 (2002).

40. E. Garcia-Garcia, A. Mendoza-Galvan, Y. Vorobiev, E. Morales-Sanchez, J. Gonzalez-Hernandez, G. Martinez, B. S. Chao, J. Vac. Sci. Technol. **A17**, 1805 (1999).

41. T. Ide. M. Suzuki, M. Okada, Jpn. J. Appl. Phys. **34**, L529 (1995).

42. Z. Sun, S. Krysta, D. Music, R. Ahuja, J. M. Schneider, Solid State Communications **143**, 240 (2007).

43. S. Yamanaka, S. Ogawa, I. Morimoto, Y. Ueshima, Jpn. J. Appl. Phys. **37**, 3327 (1998).

44. M. Niato, M. Ishimaru, Y. Hirotsu, M. Takashima, J. Non-Cryst. Solids **354&346**, 112 (2004).

45. V. Weidenhof, I. Friedrich, S. Ziegler, M. Wuttig, J. Appl. Phys. **86**, 5879 (1999).

46. Yu Jin Park, Jeong Yong Lee, Yong Tae Kim, Appl. Surf. Sci. **252**, 8102 (2006).

47. Dohyung Kim, Sang Jun Kim, Sung-Hyuck An, Sang Youl Kim, Jpn. J. Appl. Phys. **42** 5107 (2003).

48. Sung-Hyuck An, Dohyung Kim, Sang Youl Kim, Jpn. J. Appl. Phys. **41**, 7400 (2002).

49. B. J. Kooi, W. M. G. Groot, J. Th. M. De Hosson, J. Appl. Phys. **95**, 924 (2004).

50. G. Lucovsky, J. C. Phillips, J. Non-Cryst. Solids (2008), doi:10.1010/j.jnoncrysol.2007.09.059.

Figure captions

Fig. 1. Real $\langle\varepsilon_1\rangle$ (a) and imaginary $\langle\varepsilon_2\rangle$ (b) parts of the pseudodielectric function $\langle\varepsilon\rangle$ for amorphous $Ge_2Sb_2Te_5$ thin films calculated according to Tauc-Lorentz and Cody-Lorentz models (circles: experimental data, solid lines: best-fit calculation). The inserted figures show model and experimental data agreement in the absorption onset region.

Fig. 2. Comparison of ε_2 of amorphous $Ge_2Sb_2Te_5$ thin film calculated according to Tauc-Lorentz and Cody-Lorentz models. The inserted figure shows the behavior of ε_2 in the absorption onset.

Fig. 3. Real $\langle\varepsilon_1\rangle$ (a) and imaginary $\langle\varepsilon_2\rangle$ (b) parts of the pseudodielectric function $\langle\varepsilon\rangle$ for crystalline $Ge_2Sb_2Te_5$ thin films calculated according to Tauc-Lorentz + Gaussian oscillator (circles: experimental data, solid lines: best-fit calculation).

Fig. 4. The calculated real ε_1 (a) and imaginary ε_2 (b) part of dielectric function of amorphous and crystalline $Ge_2Sb_2Te_5$ thin films. The inserted pictures show the corresponding refractive index and extinction coefficient.

Fig. 5. Tauc plots: $(\alpha E)^{1/2}$ - E_g^{opt} = 0.48 eV and $(\alpha E)^2$ - E_g^{opt} = 1.67 eV as function of photon energy E (~ 195 nm, crystallized $Ge_2Sb_2Te_5$).

Fig. 6. Difference between experimental and modeled data of (a) amorphous - Tauc-Lorentz, (b) amorphous - Cody-Lorentz and (c) crystalline - Tauc-Lorentz + Gaussian oscillator $Ge_2Sb_2Te_5$ thin films.

Fig. 7. Difference between experimental and modeled data of amorphous $Ge_2Sb_2Te_5$ calculated according to Tauc-Lorentz and Cody-Lorentz models in the absorption onset region. (a) $\Delta\langle\varepsilon_1\rangle$, (b) $\Delta\langle\varepsilon_2\rangle$.

Fig. 8. XRD spectra of as-prepared (amorphous) and thermally crystallized $Ge_2Sb_2Te_5$ thin films. The *hkl* parameters of crystalline phase are assigned according to Ref. 24.

Fig. 9. Detection of phase change transition in $Ge_2Sb_2Te_5$ thin films upon different heating rates using single wavelength ellipsometry. Only heating rates 1 °C/min, 2.5 °C/min and 5 °C/min are plotted.

Fig. 10. The calculated refractive index change during the crystallization according to Fig. 9 and the derivation plot of *dn/dT*.

Fig. 11. The shift of the optical bandgap energy E_g^{opt} in dependence on temperature. The E_g^{opt} has been calculated according to Tauc-Lorentz model (amorphous phase) and Tauc-Lorentz + one Gaussian oscillator (crystalline phase).
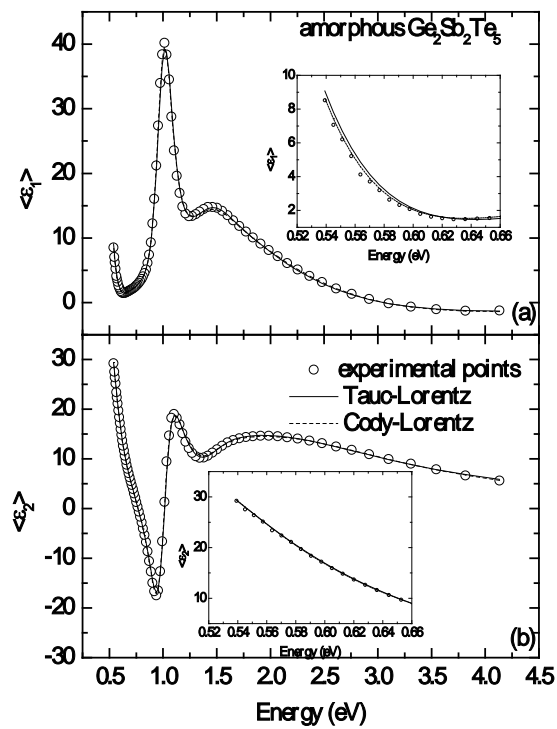
Fig. 1.
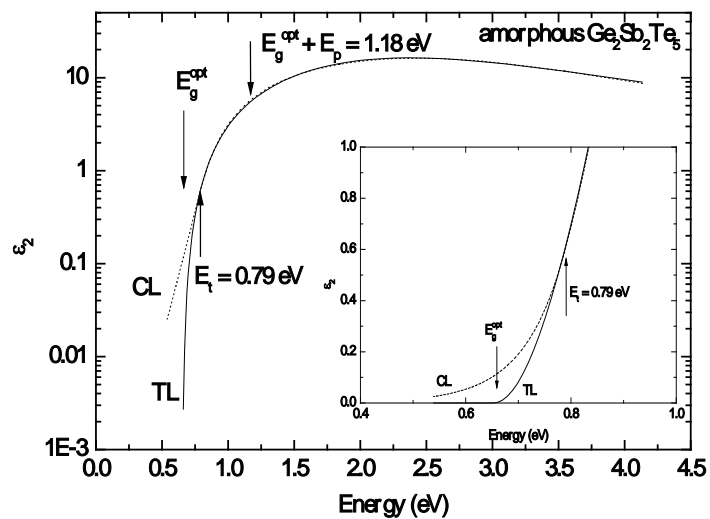
Fig. 2.
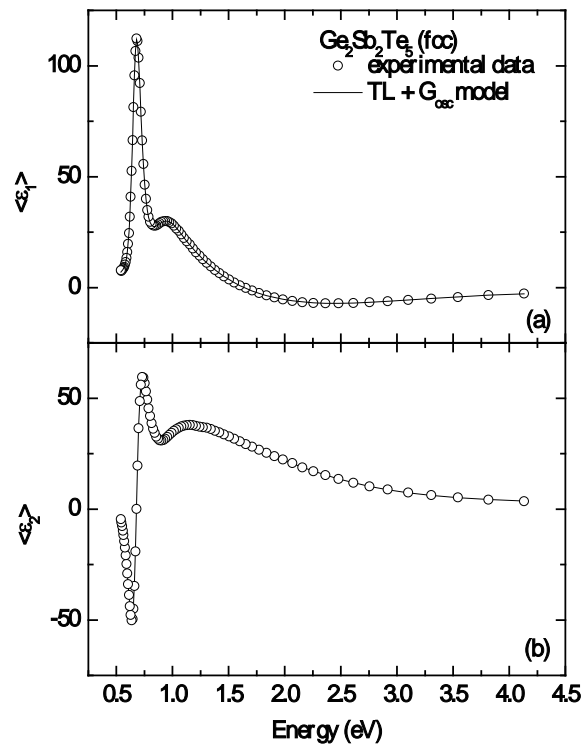
Fig. 3.
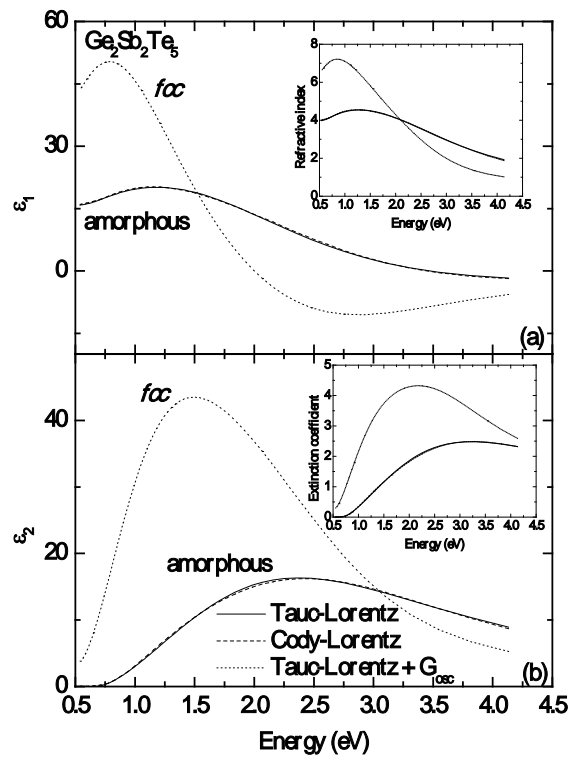
Fig. 4.
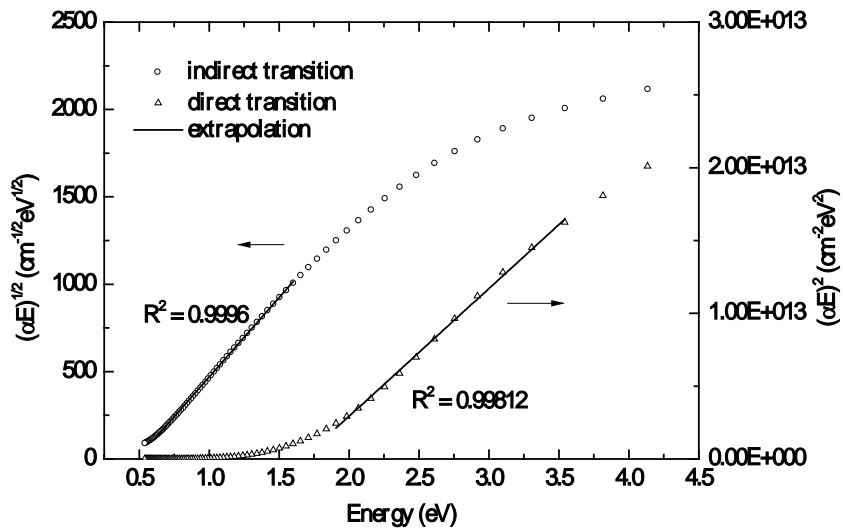
Fig. 5.
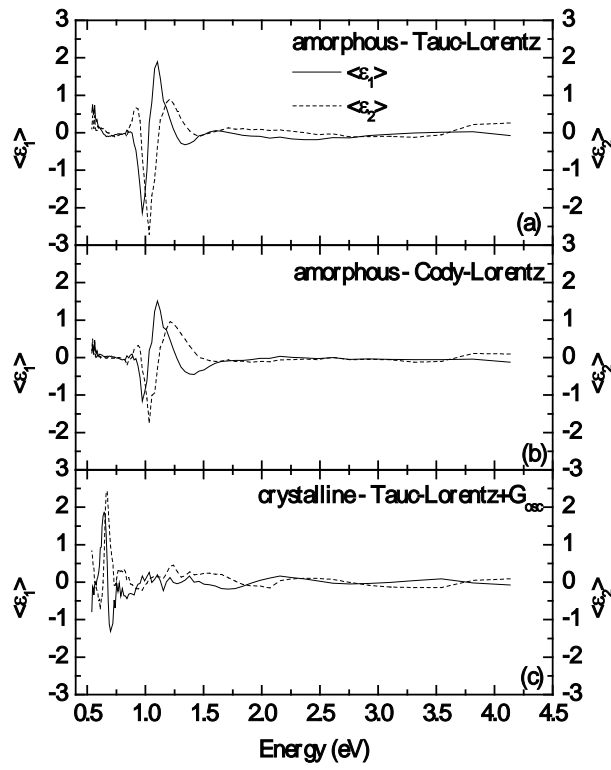
**Fig. 6.**
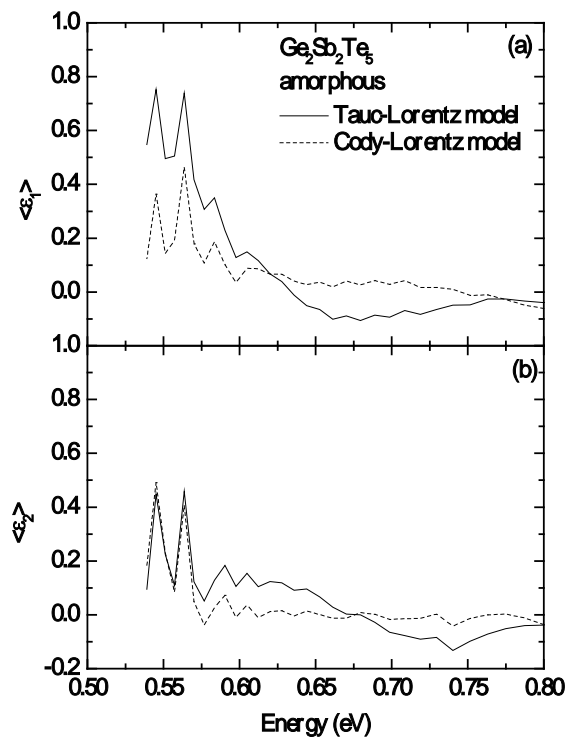
Fig. 7.
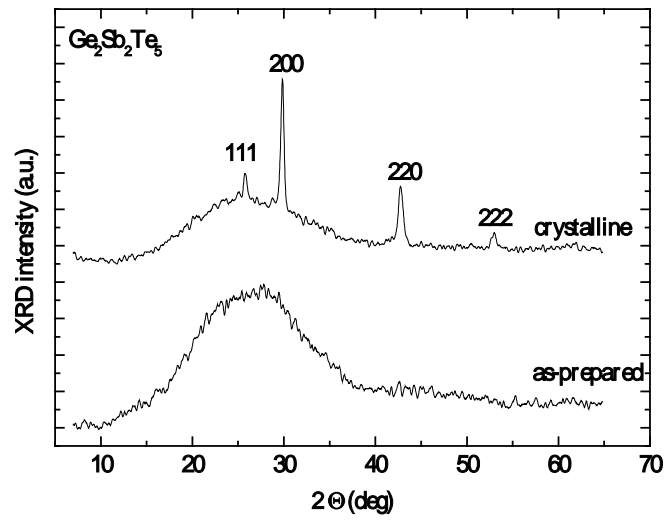
Fig. 8.
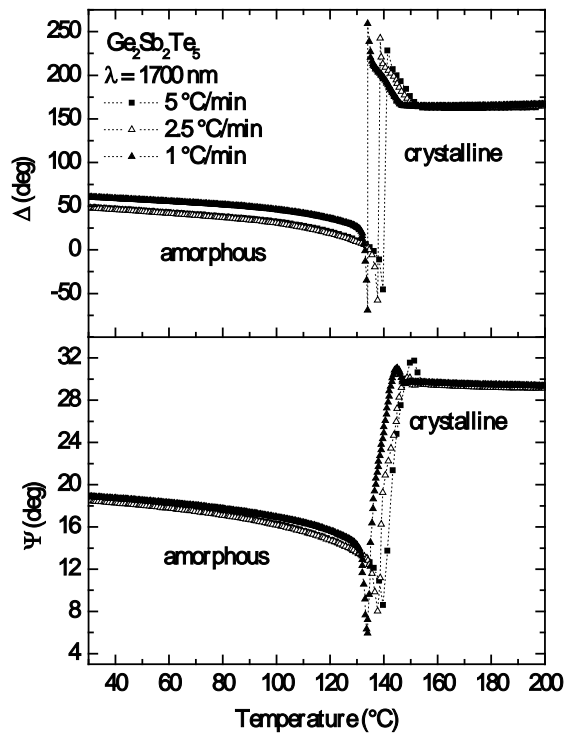
Fig. 9.
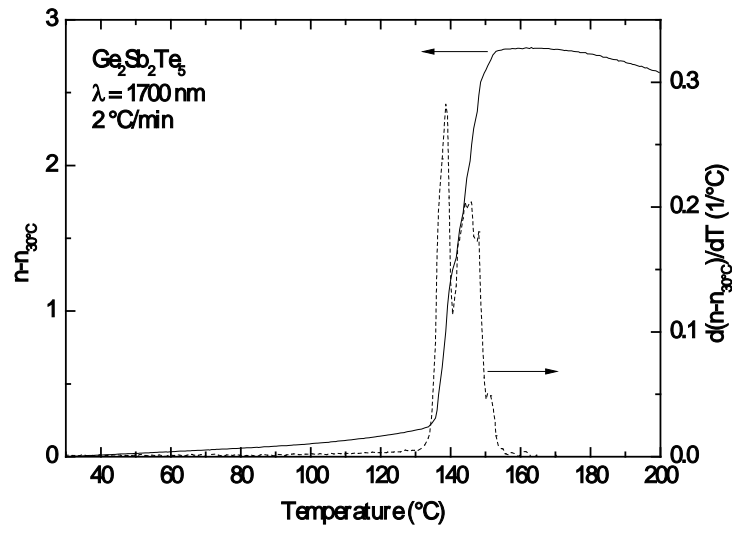
**Fig. 10.**
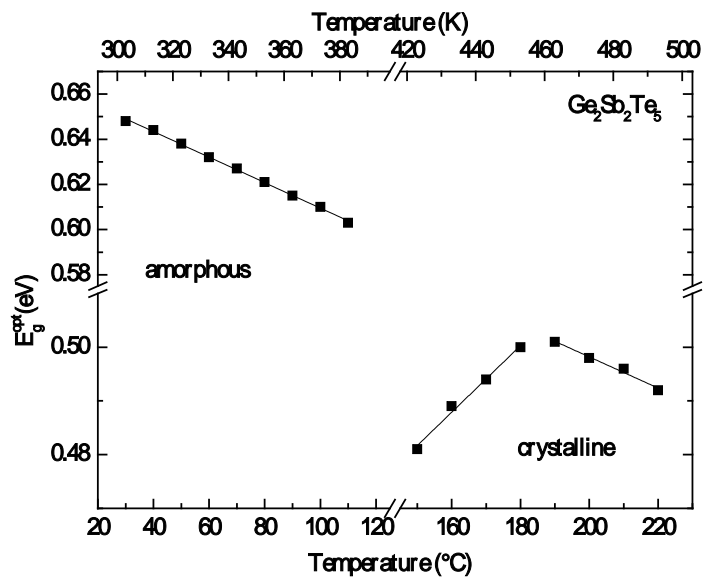
Fig. 11.

Tables

Tab. 1. Tauc-Lorentz, Cody-Lorentz and Gaussian models parameters of the studied amorphous and crystallized Ge$_2$Sb$_2$Te$_5$ FE thin films. *A (A$_G$)*, *C (C$_G$)*, *E$_0$ (E$_G$)*, *E$_g$^{opt}* represent oscillator parameters: amplitude, peak transition energy, broadening and optical bandgap energy. *E$_u$* - Urbach energy, *E$_t$* and *E$_p$* first and second transitions in CL model. *ε$_1$(∞)* is a constant contribution to the real part of dielectric function at higher energies.

Tab. 1.

	as-prepared Ge$_2$Sb$_2$Te$_5$ (amorphous)		Ge$_2$Sb$_2$Te$_5$ (*fcc*)
	Tauc-Lorentz	**Cody-Lorentz**	**TL+G$_{osc}$**
MSE	2.476	1.937	0.998
d$_{rough}$ (nm)	6.0 ± 0.1	6.0 ± 0.1	7.5 ± 0.1
d$_f$ (nm)	195.3 ± 0.2	194.5 ± 0.2	181.1 ± 0.1
A (eV)	114 ± 1	64 ± 1	181 ± 2
C (eV)	3.91 ± 0.04	4.01 ± 0.05	2.13 ± 0.02
E$_0$ (eV)	2.55 ± 0.01	2.93 ± 0.01	1.32 ± 0.01
E$_g^{opt}$ (eV)	0.65 ± 0.01	0.63 ± 0.01	0.53 ± 0.01
E$_p$ (eV)	-	0.55 ± 0.01	-
E$_t$ (eV)	-	0.79 ± 0.07	-
E$_u$ (meV)	-	70 ± 3	-
A$_G$ (eV)	-	-	25 ± 1
C$_G$ (eV)	-	-	1.83 ± 0.01
E$_G$ (eV)	-	-	1.77 ± 0.01
ε$_{1\infty}$	1.53 ± 0.07	1.96 ±0.06	2.36 ± 0.04